The selective aerobic oxidative C-C bond cleavage with the high-entropy oxide (HEO)-derived multimetallic catalyst

Shaoyuan Guo [1], Xinli Tong[1,*], Jipeng Wang [1], and Hang Tang[1]

[1]*Tianjin Key Laboratory of Organic Solar Cells and Photochemical Conversion, School of Chemistry and Chemical Engineering, Tianjin University of Technology, Tianjin 300384, P. R. China; Tel: (+86)-22-60214259; E-mail address: tongxinli@tju.edu.cn; tongxli@sohu.com.*

Supplementary Information

1. The characterization of catalysts

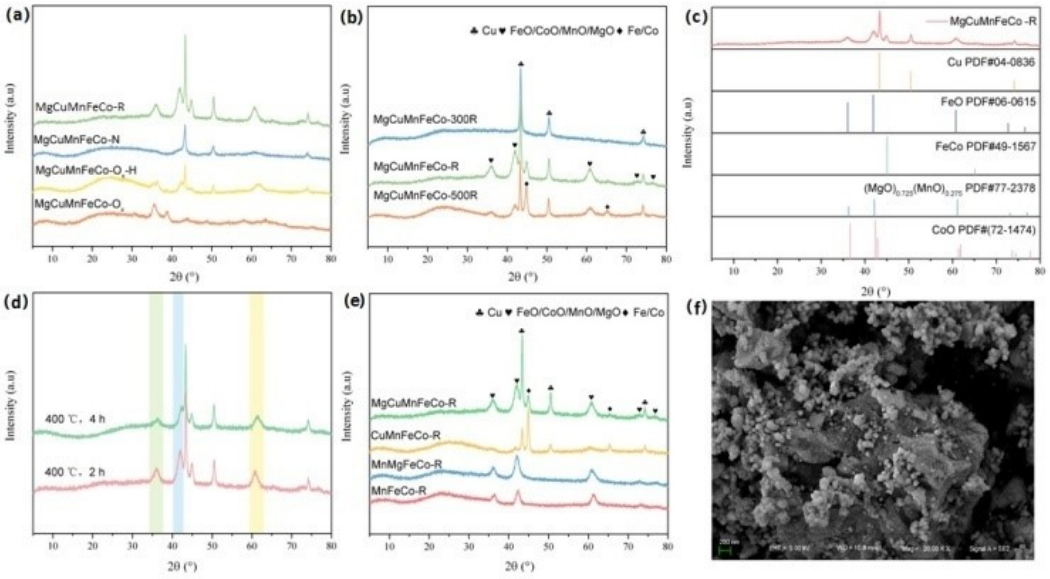

Figure S1. The XRD patterns and SEM images of the catalysts (a. XRD patterns of the catalysts with different treatments; b. XRD patterns of the catalysts with different calcination temperatures; c. PDF cards corresponding to the different elements of MgCuMnFeCo-R Catalyst; d. XRD patterns of the catalysts with different calcination times; e. XRD patterns of the catalysts with different elements; f. SEM images of the CuFeCoMnMg-R catalysts)

Table S1. The BET results of the catalysts

Catalyst	Surface Area (m^2/g)	Pore Volume (cm^3/g)	Pore Size (nm)
MgCuMnFeCo-300R	28	0.05	4.1
MgCuMnFeCo-R	80	0.09	3.5
MgCuMnFeCo-500R	52	0.11	4.2

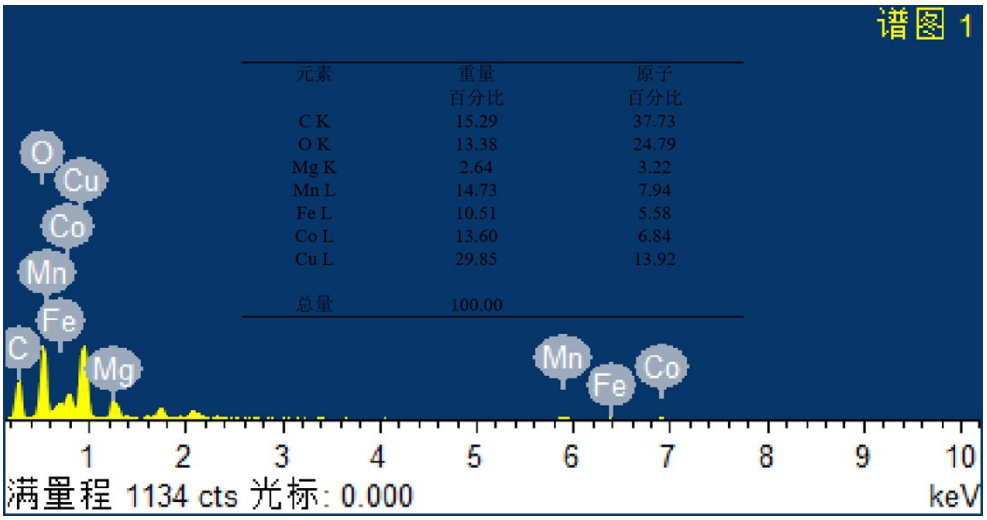

Figure S2. Energy dispersive X-ray spectroscopy (EDX) patterns of catalyst

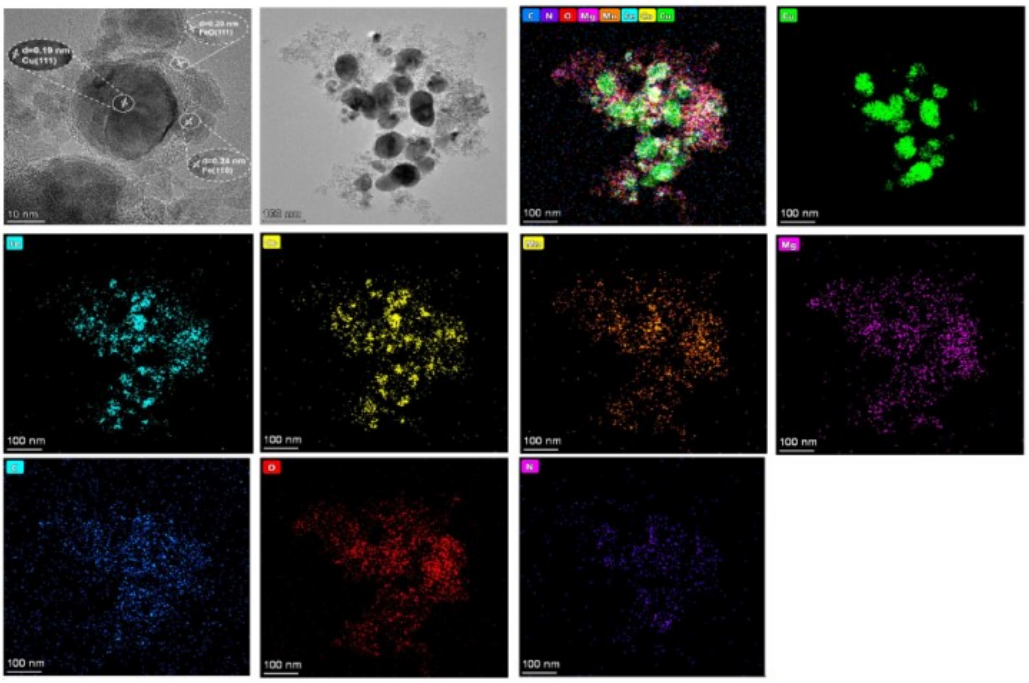

Figure S3. The TEM images and element mapping (Cu, Fe, Co, Mn, Mg, C, N, O) of the MgCuMnFeCo-R catalyst

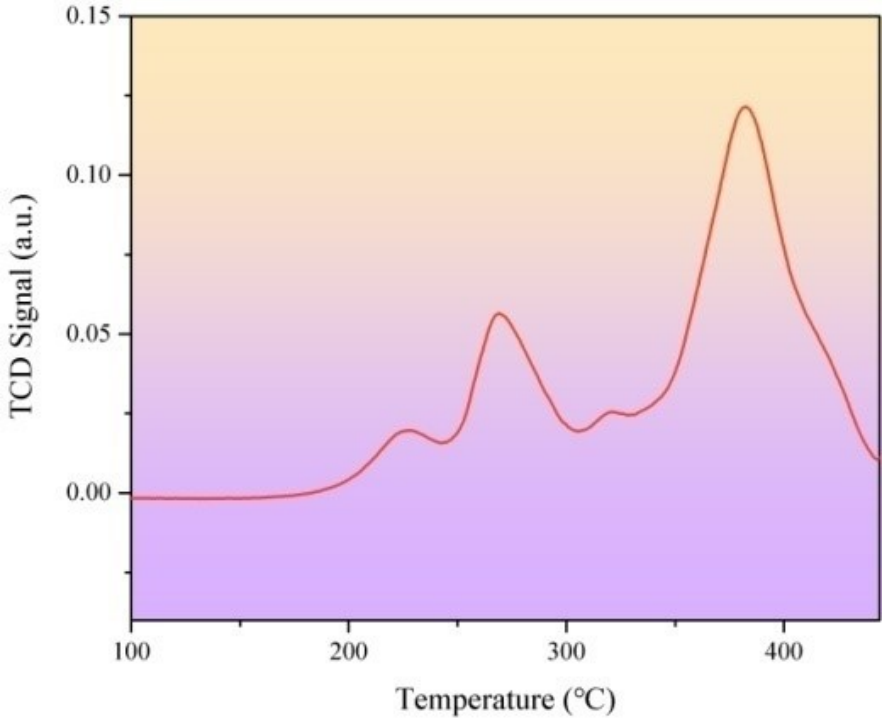

Figure S4. The result for H_2-TPR experiment of MgCuMnFeCo-P catalyst

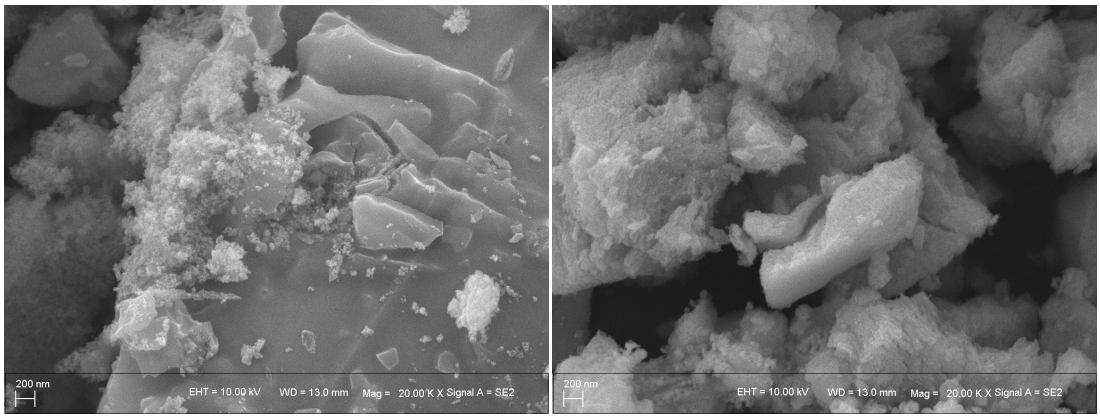

Figure S5. The SEM images of CuFeCoMnMg-O_X (left) and CuFeCoMnMg-O_X-R (right) catalyst

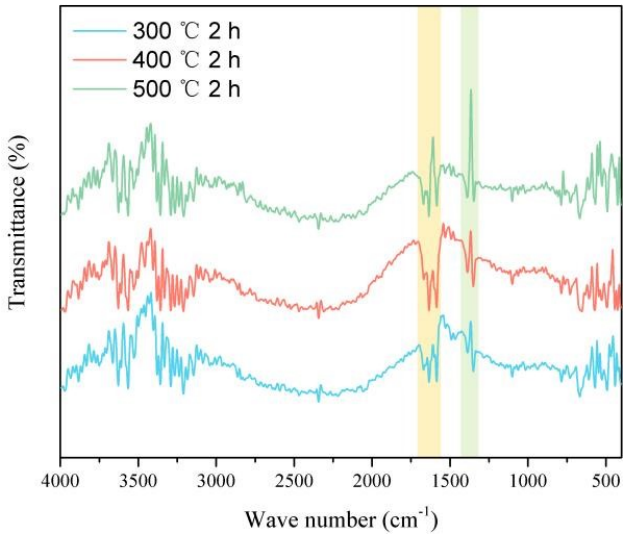

Figure S6. The IR spectra of catalysts calcined at different temperatures

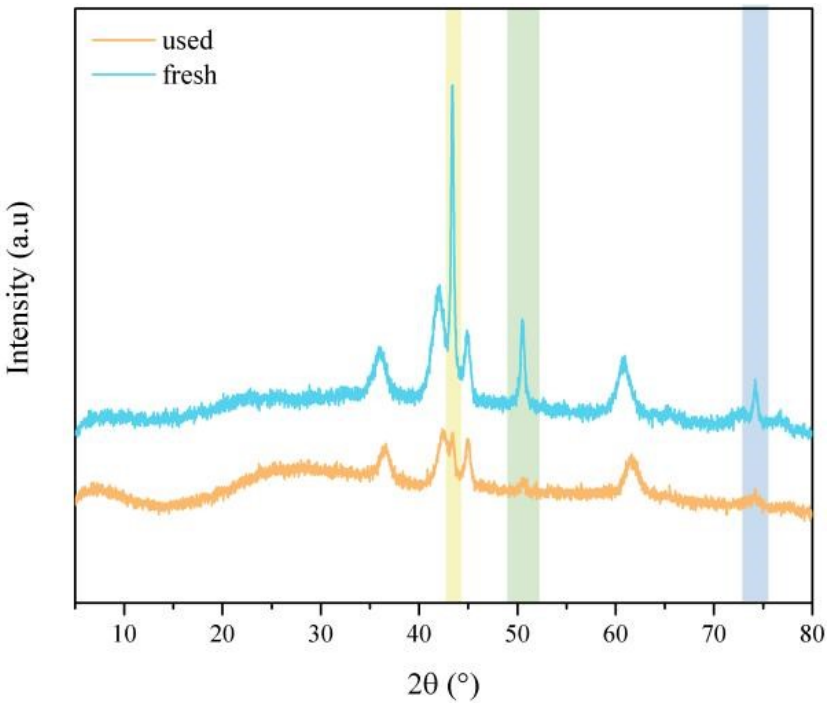

Figure S7. The XRD patterns of the fresh and reused catalysts

2. The effect of reaction solvent on the oxidative cleavage process

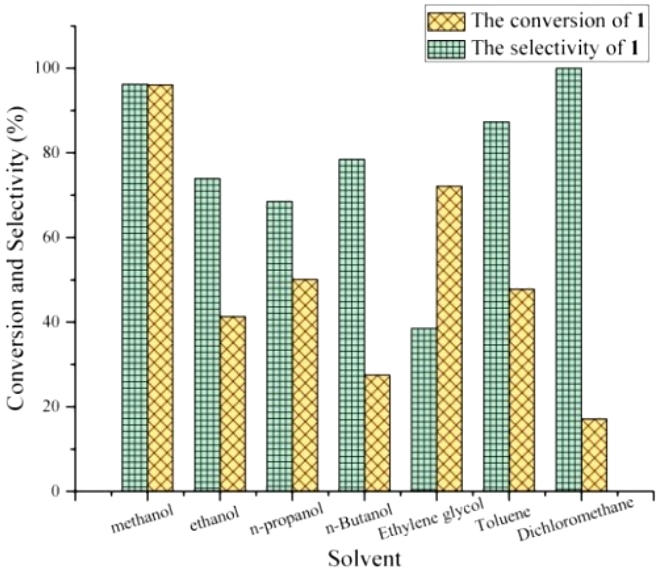

Figure S8. Effect of different solvents on oxidative cleavage process of **1** with molecular oxygen

3. The reaction mechanism of oxidation of 1 with O_2

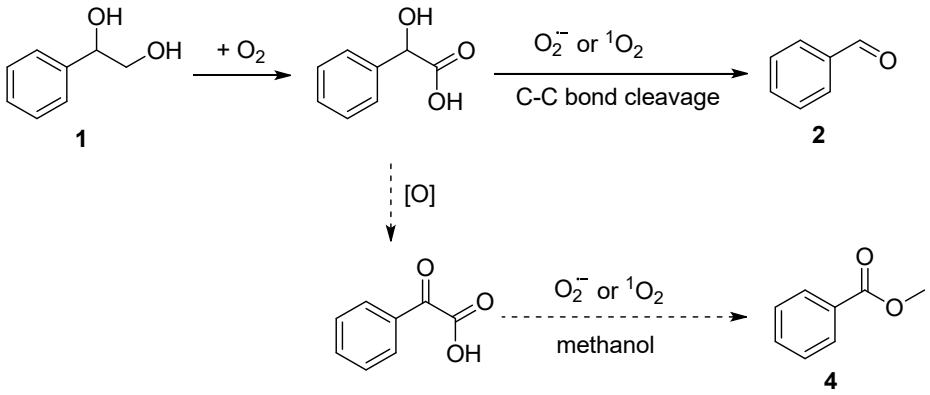

Scheme S1. The possible mechanism for the oxidative cleavage process of **1** with O_2

4. The GC and GC-MS spectra for the selective oxidative cleavage processes

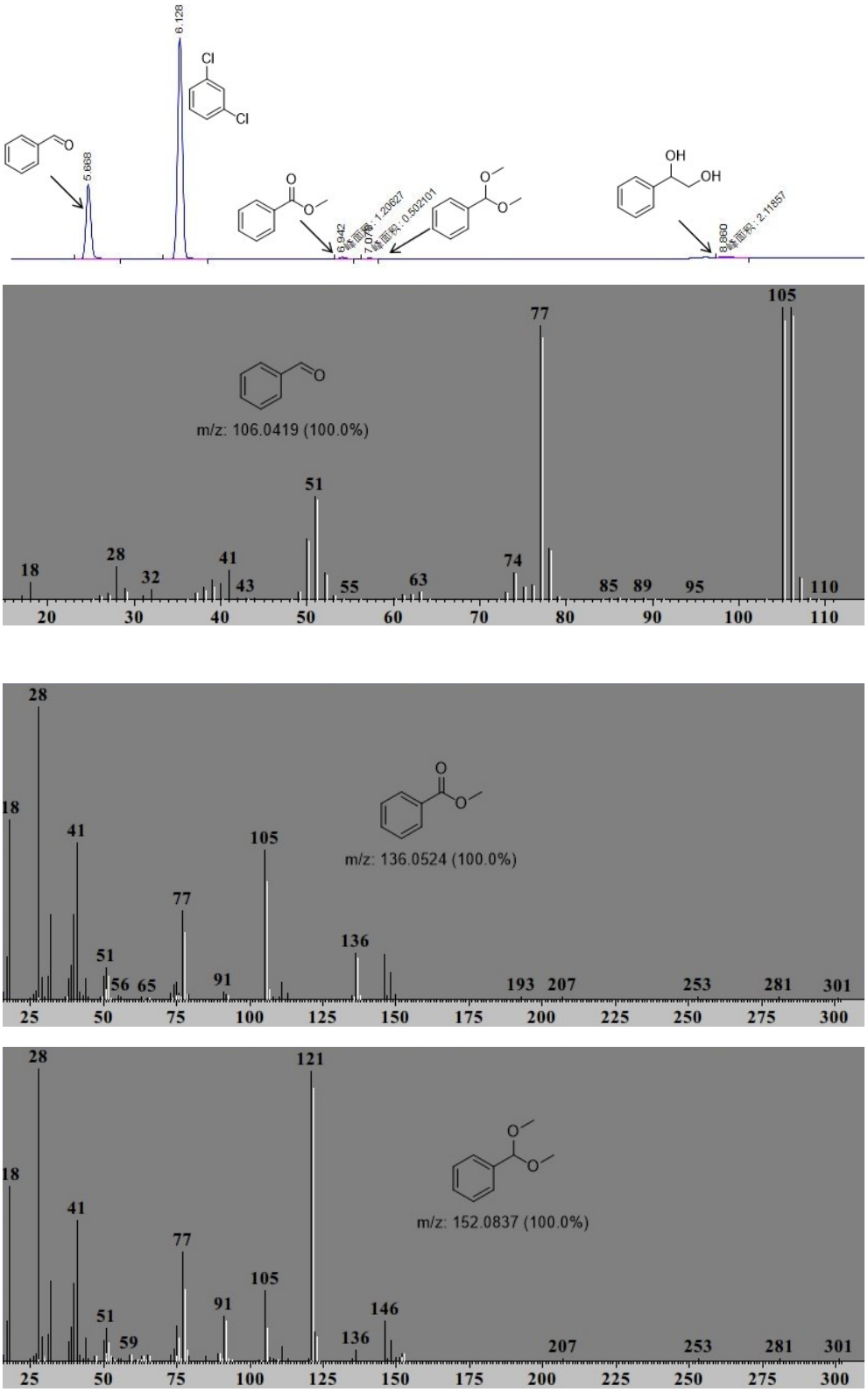

Figure S9. The GC and GC-MS spectra for reaction of 1-phenyl-1,2-ethanediol in the methanol

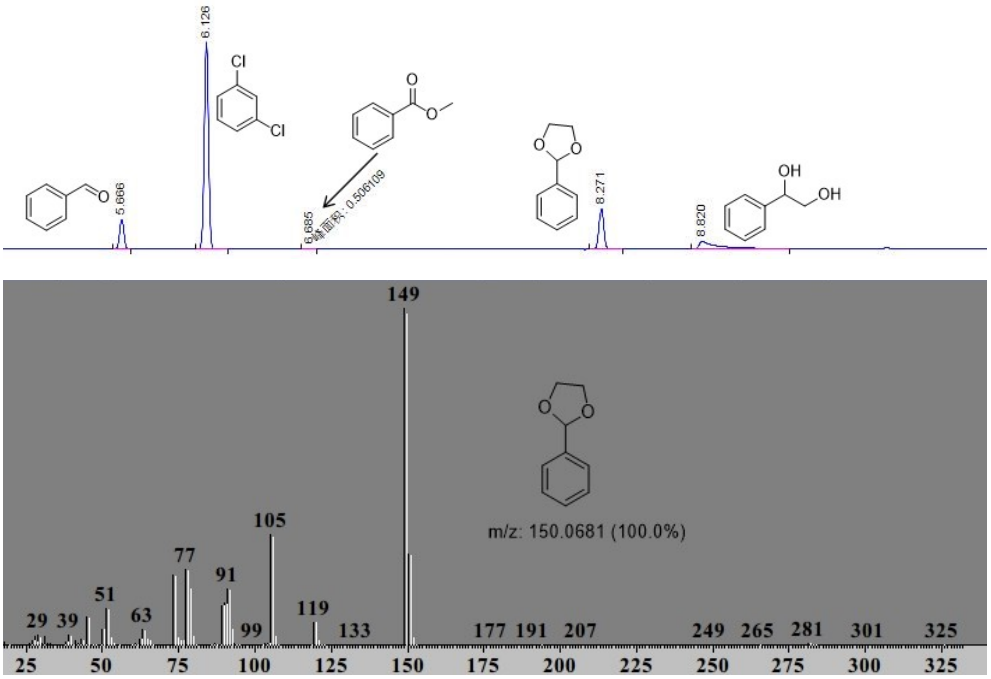

Figure S10. GC and GC-MS spectra of reaction of 1-phenyl-1,2-ethanediol in the ethylene glycol

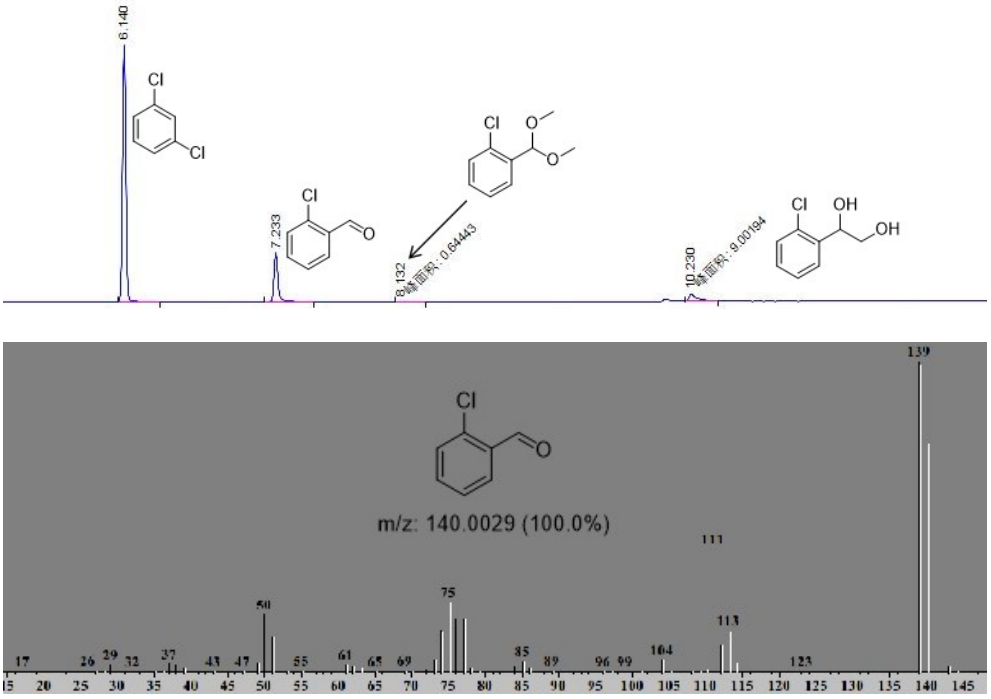

Figure S11. The GC and GC-MS spectra for the reaction of 1-(2-chlorophenyl) ethane-1, 2- diol

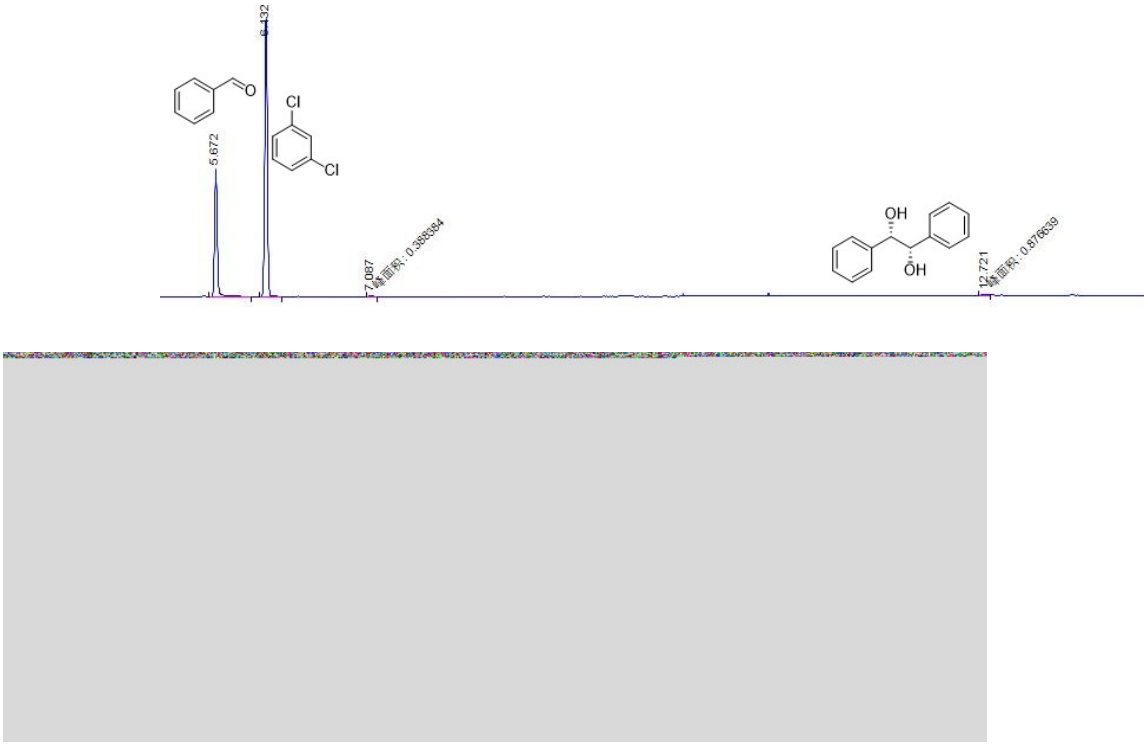

Figure S12. The GC and GC-MS spectra for the reaction of (S,S)-(-)-hydrobenzoin with O_2

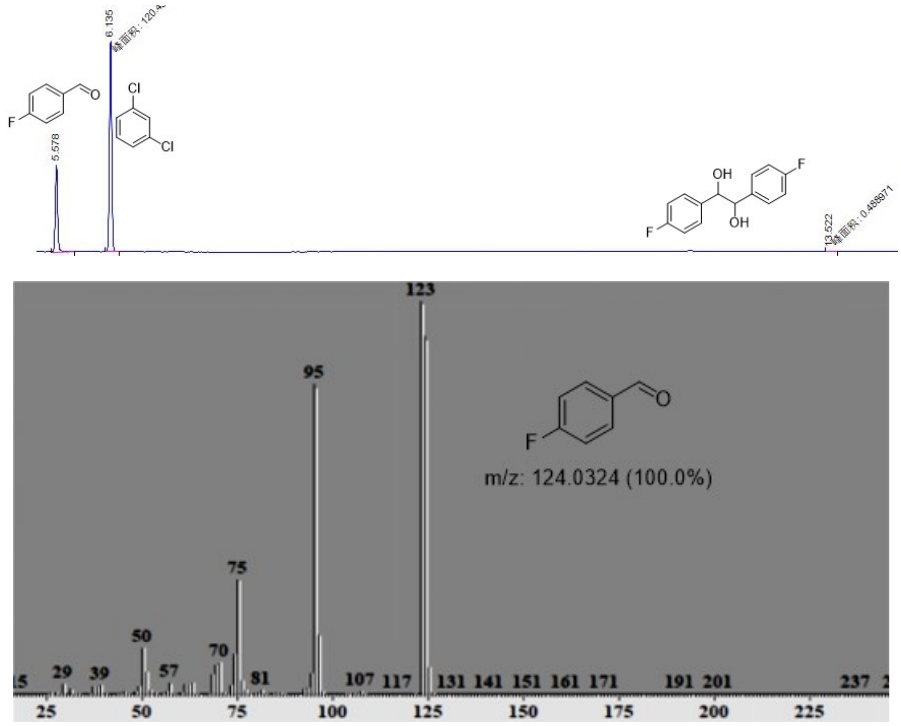

Figure S13. The GC and GC-MS spectra for reaction of 1,2-bis(4-fluorophenyl)ethane-1,2-diol

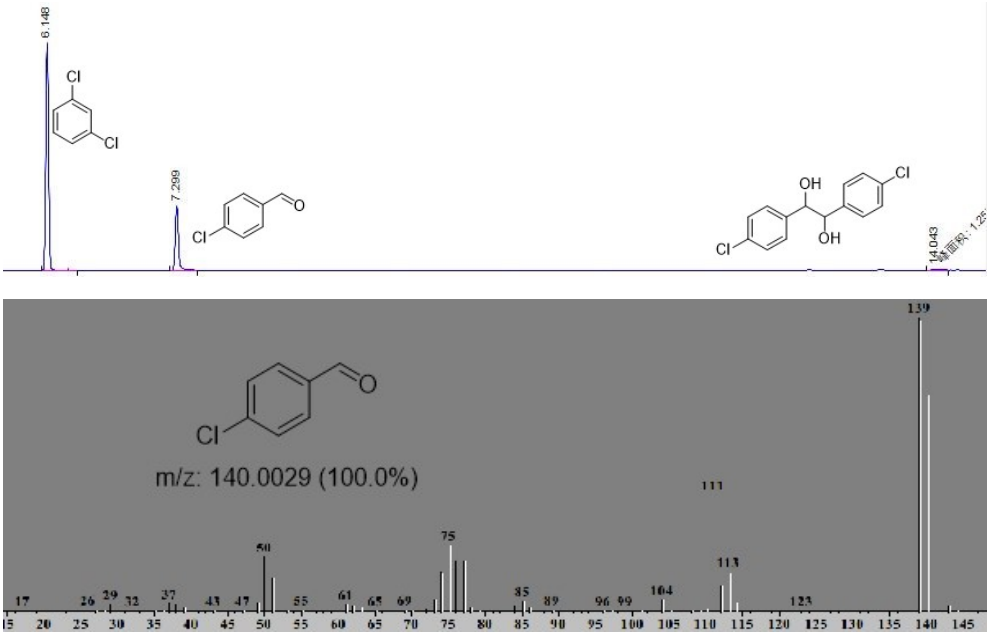

Figure S14. The GC and GC-MS spectra of reaction of 1,2-bis(4-chlorophenyl)ethane-1,2-diol

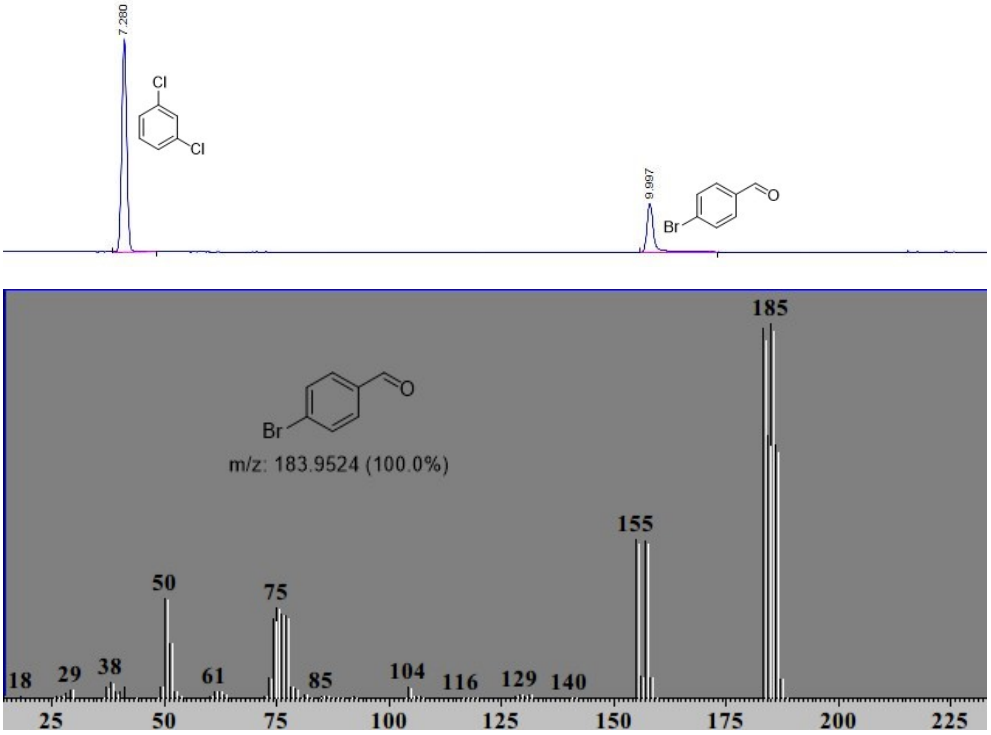

Figure S15. The GC and GC-MS spectra for reaction of 1,2-bis(4-bromophenyl)ethane-1,2-diol

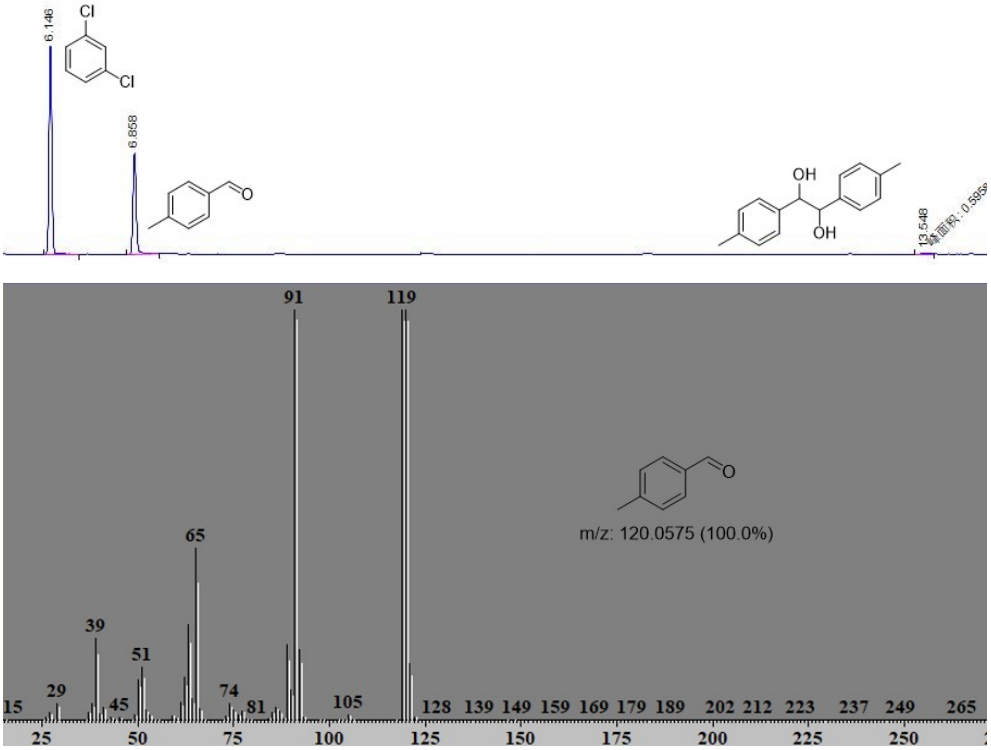

Figure S16. The GC and GC-MS spectra for reaction of 1,2-bis(4-bromophenyl)ethane-1,2-diol

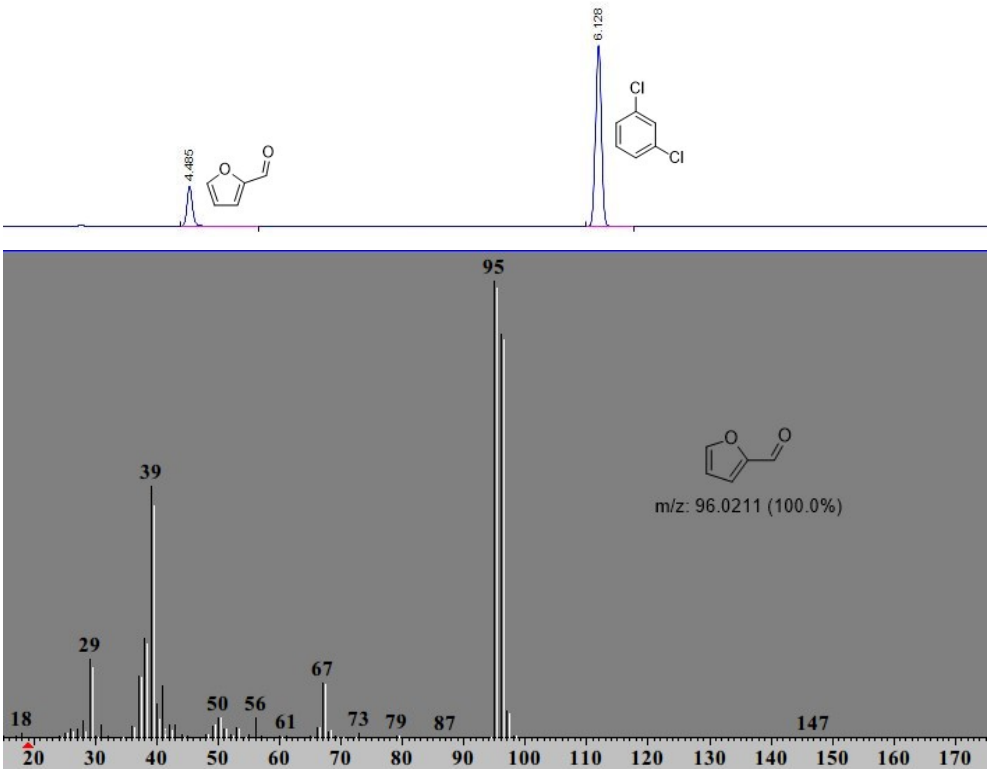

Figure S17. The GC and GC-MS spectra for the reaction of 1,2-bis(2-furanyl)ethane-1,2-diol

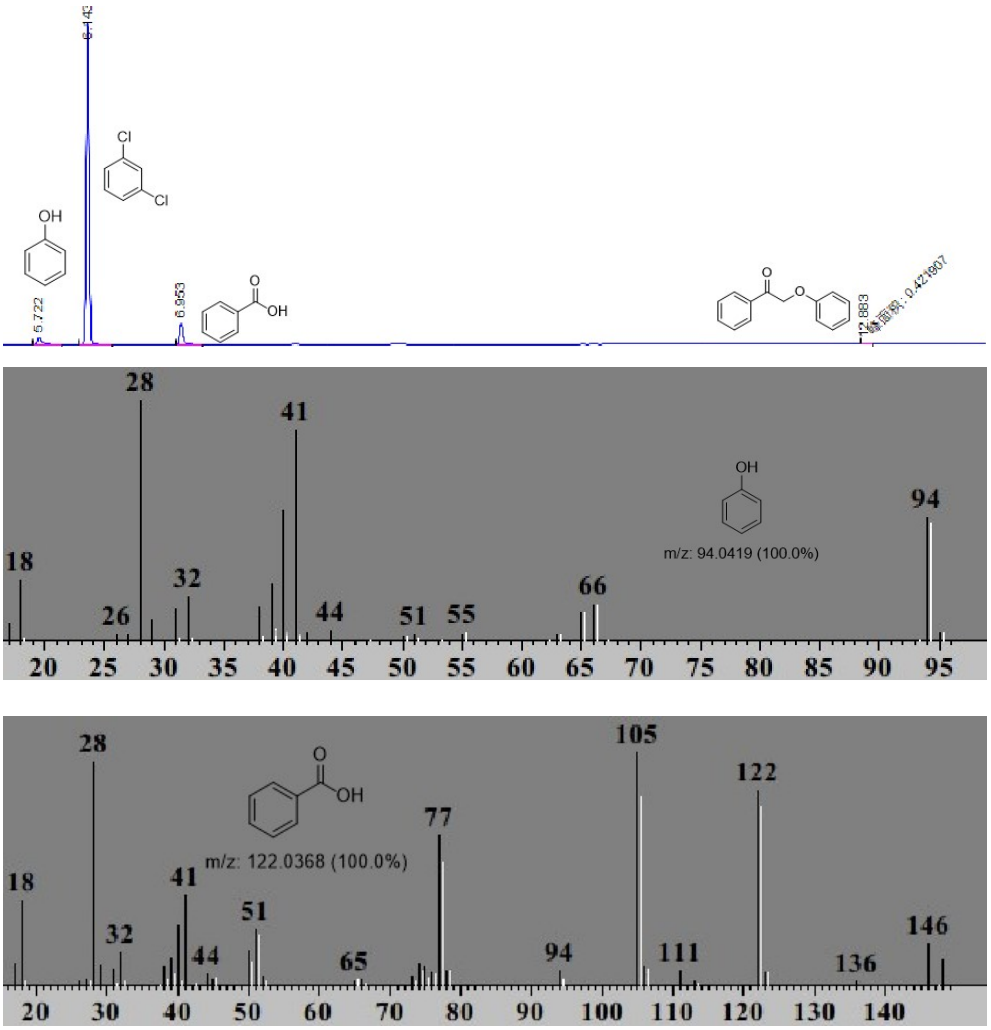

Figure S18. The GC and GC-MS spectra of reaction of 2-phenoxy-1-phenylacetophenone with O_2